Chinese Chemical Letters 35 (2024) 108880

Contents lists available at ScienceDirect

Chinese Chemical Letters

journal homepage: www.elsevier.com/locate/cclet

Quantitative detection of citrate for early stage diagnosing of prostate cancer: Discriminating normal to cancer in prostate tissues

Selvaraj Muthusamy[a,1,*], Kanagaraj Rajalakshmi[a,1], Palanisamy Kannan[b,*], Yun-Sik Nam[c], Dongwei Zhu[d], Yeonggil Seo[e], Jong-Won Song[e], Dong Nyoung Heo[f], Il Keun Kwon[f], Yuanguo Xu[a,*]

[a] School of Chemistry and Chemical Engineering, Jiangsu University, Zhenjiang 212013, China
[b] College of Biological, Chemical Sciences and Engineering, Jiaxing University, Jiaxing 314001, China
[c] Advanced Analysis Center, Korea Institute of Science & Technology, Seongbuk-gu, Seoul 02792, Republic of Korea
[d] School of Medicine, Jiangsu University, Zhenjiang 212013, China
[e] Department of Chemistry Education, Daegu University, Gyeongsan-si, Gyeongsangbuk-do 38453, Republic of Korea
[f] Department of Dental Materials, School of Dentistry, Kyung Hee University, Seoul, Republic of Korea

ARTICLE INFO

Article history:
Received 31 January 2023
Revised 19 July 2023
Accepted 1 August 2023
Available online 5 August 2023

Keywords:
Prostate cancer
Biomarker-citrate
Boronic acid
Lewis acid/base-ICT
Red-emissive
Mitochondria targeting
Prostate tissue

ABSTRACT

Prostate cancer (PC) biomarker-citrate detection is clinically important to diagnose PC in early stages. Methylquinolinium iodide (**Q**) conjugated indole-phenylboronic acid (**IB**) was designed as a red-emissive **QIB** probe for the detection of citrate through Lewis acid–base reaction and intramolecular charge transfer (ICT) sensing mechanisms. Boronic acid acts as Lewis acid as well as citrate (Lewis base) recognition unit. The probe reacted with citrate, showing enhanced red emissions. Since the probe has excellent water solubility and great biocompatibility, practical application in biological systems is possible. Citrate was monitored precisely in the mitochondria organelle (*in vitro*) of living cells with a positive charge on **QIB**. Also, endogenous (*in situ)* citrate was detected quantitatively to discriminate non-cancerous and PC mice, observed strong and lower (negligible) emission intensity on non-cancerous and cancerous prostate tissues, respectively. Because, the concentration of citrate is higher in healthy prostate compared with PC prostate. Furthermore, the analysis of sliced prostate tissues can give PC-related information for clinical diagnosis to prevent and treat PC in the initial stages. Therefore, we believe that the present probe is a promising biochemical reagent in diagnosing PC.

Deficient citrate causes prostate cancer (PC) in men [1,2]. A prostate-specific antigen (PSA) study is performed to diagnosis PC in the early stage by examining the blood samples of patients [1–5]. The drawbacks of lacking sensitivity and poor selectivity in the elevation of the PSA levels results in a false diagnosis of PC in one among four men displaying abnormal PSA levels [1,2,5]. Therefore, an appropriate analysis method should be developed to avoid nonessential clinical tests to diagnosis PC in the early stages. Usually, a malignant prostate has a 2–20 mmol/L citrate concentration, which is much lower than that of healthy prostates (50–200 mmol/L) [1,2,6,7]. Diagnosing the concentration of citrate in biological experiments can provide PC-related signals for clinical application. The existence of citrate in mitochondria can play an essential role in the Krebs cycle, cellular energy metabolism, kidney stone disease, insulin secretion, and cancer (PC) [1,2,8–10]. Hence, monitoring citrate quantitatively in biological samples could be a potential diagnostic method [11,12].

Fluorescent chemosensors are widely employed in detecting citrate using indicator displacement assay (IDA) and non-IDA methods [1,2,13–15]. Recently, we developed two fluorophores including boronate and boronic acid to detect the PC biomarker citrate with the Lewis acid-base sensing phenomenon [1,2]. The boron atom (Lewis base) in boronate and boronic acid probes possesses an empty "p" orbital with a positive charge, including sp^2 hybridization and trigonal planar geometry [1,2]. Citrate (Lewis acid) can donate the electrons to the empty "p" orbital of the boron atom and prompt structural deformation from sp^2 trigonal planar to sp^3 tetrahedral as well as the formation of an alcohol as a final product [1,2]. Accordingly, a boronic acid-incorporated fluorophore may replace the IDA sensing strategy and overcome the metal-probe complexation. In early 2022, a rhodamine-conjugated indole-boronic

* Corresponding authors.
E-mail addresses: rajselva311@ujs.edu.cn (S. Muthusamy), ktpkannan@zjxu.edu.cn (P. Kannan), xuyg@ujs.edu.cn (Y. Xu).
[1] These authors contributed equally to this work.

https://doi.org/10.1016/j.cclet.2023.108880
1001-8417/

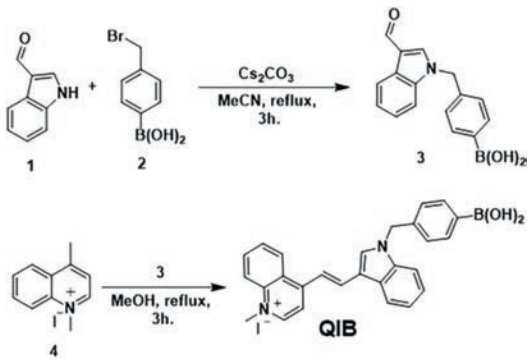

Scheme 1. Synthetic representation of **QIB**.

acid probe was developed to monitor citrate in biosamples, which secured greater water solubility and mitochondria-targeting ability [1]. However, the present work is improved to detect citrate quantitatively in bioimaging systems to diagnose PC in the early stages. Also, a 100% water-soluble fluorophore can be used in a wide range of applications in biological experiments. Indeed, quinolinium exhibits red emission, excellent water solubility, and great membrane permeability in cell lines, and so has been drawing much attention in the biosensor field [16,17].

Therefore, a red-emissive fluorophore consisting of methylquinolinium iodide (**Q**) and indole-phenylboronic acid (**IB**) was designed to fulfill the above purposes (Scheme 1). Indole was conjugated as a π-spacer between **Q** and phenylboronic acid, where boronic acid acts as a citrate recognition moiety through a straightforward reaction of a Lewis acid-base sensing mechanism. Afterwards, methylphenol was eliminated and resonance stabilized into a methylquinolinium-indole (**QI**) product on increasing citrate concentration. The probe secured a large Stokes shift of 134 nm and obtained a lower LOD value of 38 nmol/L (S/N = 3). Citrate was detected quantitatively in prostate tissue to discriminate normal and cancer-affected prostates, which can signal the importance of treatment of PC patients the early stages by virtue of the medical applications. The **QIB** probe has the properties of being 100% water soluble, with citrate recognition boronic acid, red emission, and quantitative sensing performance in bio-experiments, and it acts as a biochemical reagent in diagnosing PC.

Methylquinolinium iodide (**Q**) and indole-phenylboronic acid (**IB**) were synthesized based on previous reports [1,18,19]. The **QIB** probe was prepared by condensation of **Q** and **IB** as shown in Scheme 1, and primary characterizations were carried out using NMR and HR-MS (Figs. S3–S5 in Supporting information).

An absorption study was performed between the **QIB** probe (5 μmol/L) and citrate. The probe exhibited the maximum absorption peak at 494 nm (Fig. 1A), which decreased with each addition of citrate (1 μmol/L) up to 24 μmol/L, and the absorption peak fell down at 488 nm.

The sensitivity of the probe was investigated in the emission spectra against citrate biomolecule. The **QIB** probe (2 μmol/L) showed a weak emission at 628 nm in the presence of boronic acid upon excitation at 494 nm (Fig. 1B). The probe revealed the inhibition of intramolecular charge transfer (ICT) from methylphenylboronic acid to methylquinolinium iodide group. [20] The emission peak was enhanced and blue-shifted from 628 nm to 608 nm with the gradual addition of citrate (0.5 μmol/L) up to 5 μmol/L concentration (Fig. 1B). This strong emission is because of the structural deformation from **QIB** to **QI** product as a result of the straightforward reactions of Lewis acid-base followed by the elimination of quinone, besides the ICT-ON process [20]. The ICT process in **QIB** facilitated the electron-pulling ability between the head-terminal quinolinium and the tail-terminal indole, causing significant changes in the emission spectra as a result of strong red emission. The probe exhibited a larger Stokes shift of 134 nm. The correlation coefficient of the probe against citrate titration was found to be 0.9854 and likewise secured the lowest limit of detection (LOD) value 38 nmol/L (S/N) subject to a linear relation graph, as depicted in Fig. S6 (Supporting information). The existing probes for the detection of citrate were compared with **QIB** (Table S1 in Supporting information). The **QIB** probe showed great water solubility, excellent selectivity, high sensitivity, and the lowest LOD value in the detection of citrate.

The selectivity parameter was investigated to evaluate the performance of the probe using various interference analytes (10 mmol/L). The fluorescence response was monitored only for the citrate biomolecule, whereas other analytes failed to show significant changes in the emission spectra (Fig. S7A in Supporting information). However, the emission changes occurred remarkably with the mixtures of interference analytes and citrate (5 μmol/L) as shown in Fig. S7A, because citrate can react with **QIB** and be converted into **QI**. The effect of pH was evaluated using HCl and NaOH solutions, and the emission responses were recorded, as shown in Figs. S7C and D (Supporting information). The emission signals were nearly unchanged at various pH (3.0–10.0), which suggested that the probe is stable at various pH ranges (Fig. S7C). Including citrate, the fluorescence intensity remained constant for acidic pH (3.0–6.0). However, after the addition of citrate (5 μmol/L) to the probe solutions of pH (7.0–10.0), there was stronger emission behavior and a blue-shift from 628 nm to 608 nm was seen by reason of the Lewis acid–base reaction mechanism and development of **QI** (Fig. S7C). Therefore, all experiments were performed at physiological pH (7.0) towards citrate. Following that, the stability of the probe was evaluated using the fluorescence spectra at various time periods such as fresh solution, after 24 h, and after seven days. Accordingly, the emission peaks revealed that **QIB** has excellent stability with time (Fig. S8A in Supporting information). Also, the flu-

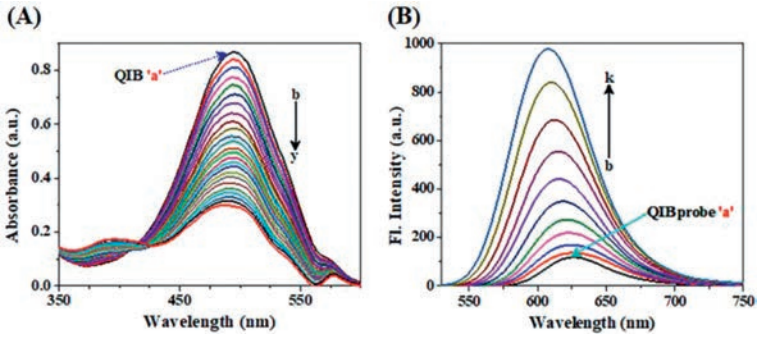

Fig. 1. UV–vis spectra obtained for 5 μmol/L **QIB** (a) with each addition of (A) 2 μmol/L citrate ("b to y"). Fluorescence emission responses for 2 μmol/L **QIB** (a) with each addition of (B) 0.5 μmol/L citrate ("b to k"), excitation at 494 nm.

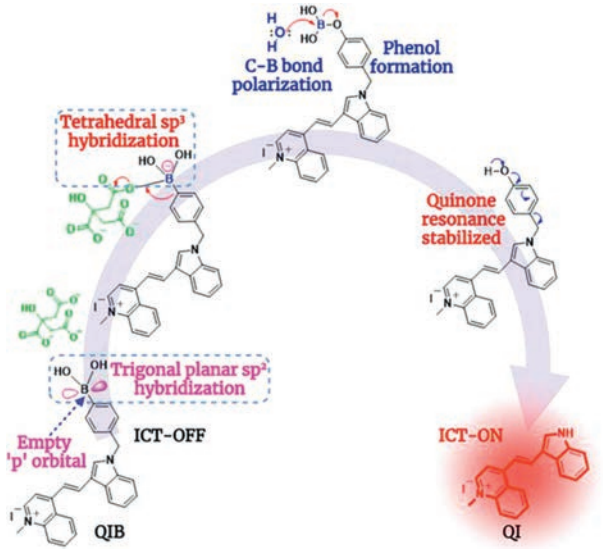

Fig. 2. Sensing mechanism of **QIB** and citrate.

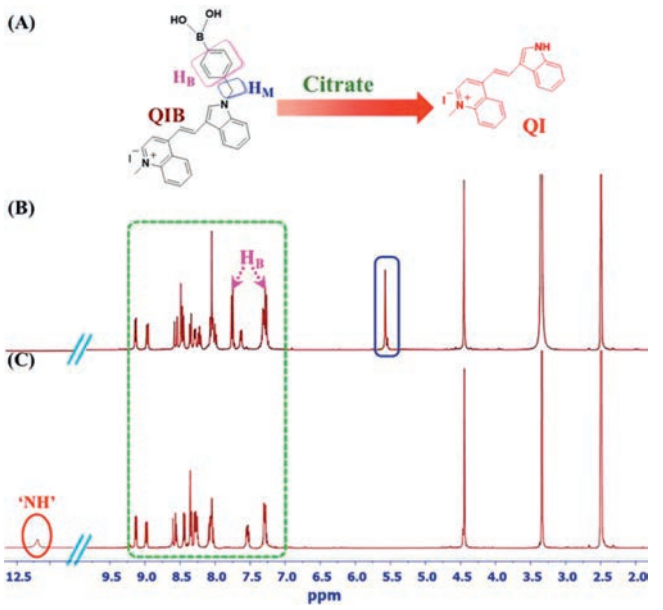

Fig. 3. (A) Conversion of **QIB** to **QI**, ^{1}H NMR spectra of the **QIB** probe (B) before and (C) after reacting with citrate.

orescence intensity of **QIB** was examined using various amounts of citrate (0, 0.5, 3.5, and 5 μmol/L) to determine the reaction time, and the enhanced emission was saturated at *ca.* 3 min (Fig. S8B in Supporting information). The fluorescence quantum yield of the probe was determined as 0.49 and 0.80 before and after reaction with citrate, respectively (Table S2 in Supporting information).

The Lewis acid–base reaction between **QIB** and citrate was evaluated through the emission spectra (Fig. 1). Also, ^{1}H NMR and HR-MS titration experiments were performed to verify the proposed sensing mechanism, as shown in Fig. 3, Figs. S3, S5 and S9 (Supporting information). The **QIB** probe exhibited a weak emission peak at 628 nm, which gradually increased with every addition of citrate up to 5 μmol/L, along with a blue shift from 628 nm to 608 nm (Fig. 1). This was because the boronic acid in the **QIB** probe was modified to corresponding indole product of **QI**, caused by the Lewis acid–base reaction followed by a quinone resonance stabilized structure. Boron atom in boronic acid has an empty "p" orbital, which acts as Lewis acid and readily accepts the electrons from citrate (Lewis base) (Fig. 2) [1,2]. It is a well-known fact that boron in boronic acid possesses a trigonal planar with sp^2 hybridization geometry, which converts to tetrahedral sp^3 hybridization after accepting the electrons from citrate. In fact, the carbon–boron (C–B) bond was polarized and formed an alcohol product of **QI-OH**. Surprisingly, the basicity of citrate induced the quinone structure and resonance stabilized into **QI** as well as enhanced red emission with the ICT-ON process (Figs. 2 and 3). These structural alterations were shown in ^{1}H NMR and HR-MS with proton appearance/shifts, and mass value differences, respectively (Fig. 3 and Fig. S9). The phenylboronic acid (pink arrows-H_B) and methylene (blue box-H_M) protons of **QIB** disappeared at δ values of 7.74, 7.26, and 5.56, ppm, respectively, as shown in Fig. 3. Also, an "NH" proton appeared at δ = 12.14 ppm (red circle) due to newly formed methylquinolinium iodide-indole (**QI**) (Fig. 3C). After being titrated with citrate, the aromatic protons of methylquinolinium iodide and indole shifted up- and down-field, as depicted in the green dotted box (Figs. 3B and C). These structural conversions were again confirmed through HR-MS *m/z*: calculated for $C_{20}H_{17}N_2$, $[M\text{-}I]^+$ = 285.1386, and found $[M\text{-}I]^+$ = 285.1459 (Fig. S9).

DFT calculations were performed to predict the minimum-energy conformations of **QIB, QI**, and **QI-OH** theoretically to understand the origin of the spectral variations among the **QIB**, **QI**, and **QI-OH** at the molecular level (Fig. 4). The experimental UV–vis spectral changes within the **QIB** and **QI** were identical to the calculated results (Figs. 1 and 4). In detail, the calculated spectrum of **QIB** has a peak in slightly longer than 500 nm region, but that of **QI** has a peak in slightly less than 500 nm region with weakened intensity compared with **QIB**, which coincides with the experimentally observed UV–vis absorption spectra (Figs. 1 and 4). However, we reason that quinone cleavage takes place soon, since the calculated UV–vis spectrum of **QI-OH** does not show either weakened intensity or a slight blue-shift of the peak near 500 nm (Fig. 4C). Moreover, both a slight blue-shift and slight strengthened intensity of the peak near 300 nm in the reaction were also seen in the theoretical UV–vis spectra at the molecular level. An investigation of molecular orbitals related to the electronic transition showed that the main origin of the peak near 500 nm is a local electronic transition between the molecular orbitals on methylquinolinium iodide, and the changed chemical environment, such as eliminated methylphenyl boronic acid, is expected to result in UV–vis spectral changes (Fig. 4) [1,21–23].

QIB was employed to evaluate the level of citrate in urine samples, which were collected from different people. To investigate the lower concentration of citrate, the urine samples were diluted 100 times with distilled water, then treated with the **QIB** probe (0.5 mmol/L) solution to determine the amount of citrate in the urine samples. The efficiency of the probe was investigated in determining the noted amounts of citrate. The fluorimetric and HPLC results were compared as shown in Table S3 (Supporting information). The relative standard deviation (RSD) was calculated with measurements of urine samples repeated five times (n = 5). The fluorimetric sensing and HPLC methods were used together to evaluate the concentration of citrate in the urine samples. An MTT assay was conducted to evaluate the biocompatibility of **QIB** with PC3 cells. The cell survivability was found to be >85% using 200 μmol/L of **QIB** in PC3 live cells (Fig. S10 in Supporting information). Next, the fluorescence imaging of **QIB** in detecting citrate was tested. A control experiment was carried out in PC3 cells before incubation of the probe solutions for reference (Figs. 5A–C). The cells were incubated with **QIB** (2 μmol/L) for nearly 30 min, and weak red emission was observed as shown in Figs. 5D–F. The addition of citrate (2.5 μmol/L) to the pre-treated cells showed a moderate red fluorescence (Figs. 5G–I). On increasing the amount

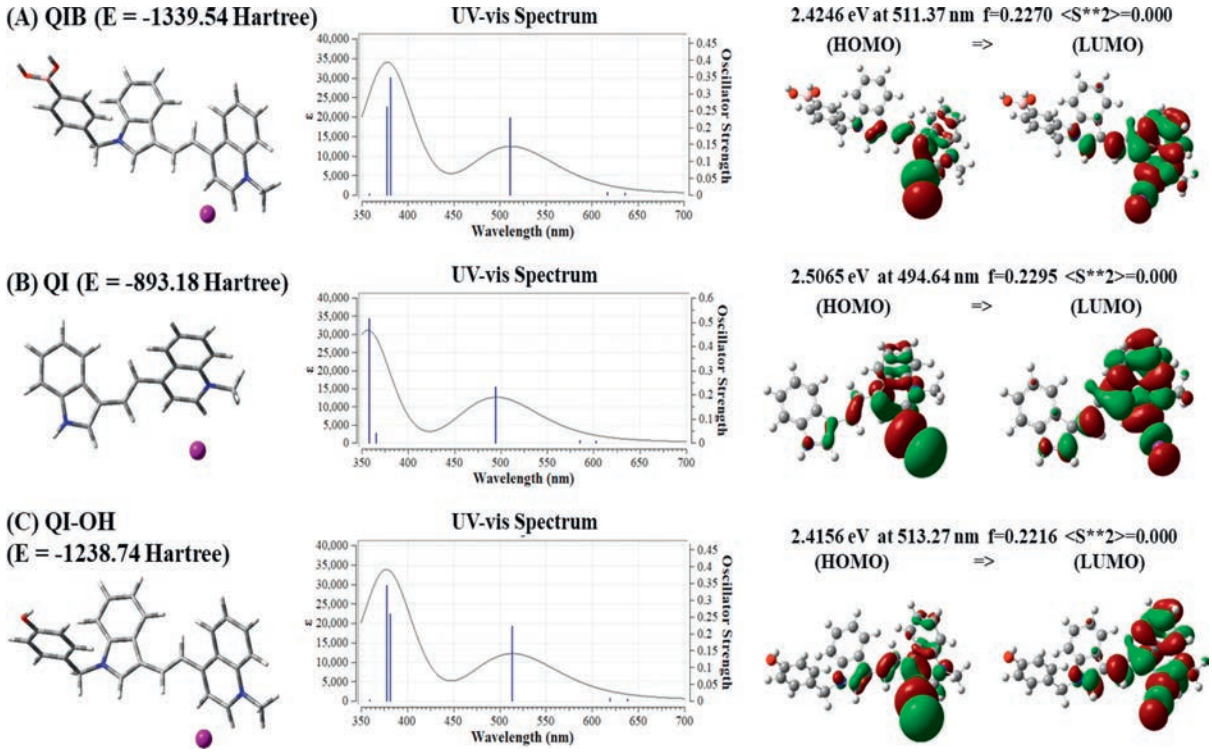

Fig. 4. Optimized structures and their energies (Hartree) of (A) **QIB**, (B) **QI** and (C) **QI**-OH, their UV–vis absorption spectra, and their molecular orbital shapes related to the electronic transitions corresponding to the main peaks near the 500 nm region.

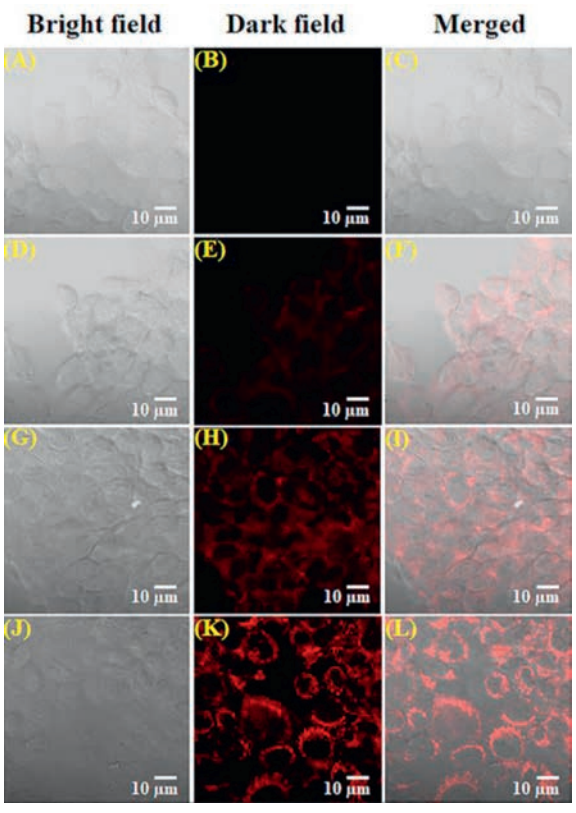

Fig. 5. Confocal images of PC 3 cells. (A–C) representation of control tests of cells; (D–F) incubated with **QIB** (2 μmol/L) nearly 30 min. The probe pre-treated cells with citrate (G–I) 2.5 μmol/L and (J–L) 5 μmol/L.

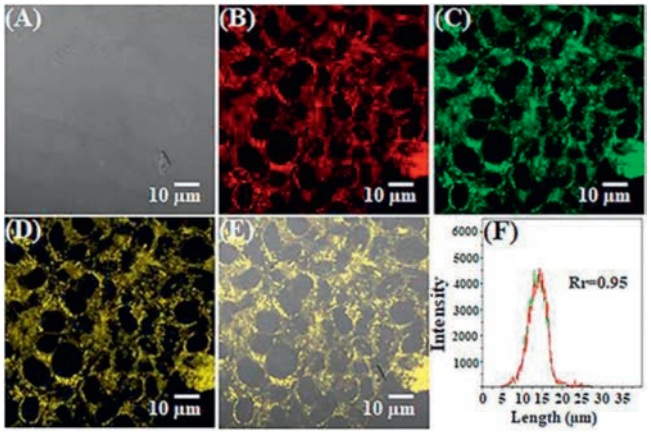

Fig. 6. Confocal images obtained for (A) **QIB**-bright-field, (B) probe pre-treated cells reacted with 5 μmol/L citrate, (C) Mito-tracker dye, (D, E) overlapping images, and (F) fluorescence intensities of the red and green interest areas in (B, C).

of citrate (5 μmol/L) in the probe-treated cells, the cell images exhibited an intense red emission (Figs. 5J–L).

After the cell images were observed with the dotted red emissions (Fig. 5), the mitochondria targeting ability of **QIB** was investigated for the detection of citrate using Mito-Tracker Green dye for reference (Fig. 6) [1]. The **QIB** probe was mixed with citrate and included Mito-targeting dye, showing green fluorescence images for the reference dye in the green channel and a red fluorescence image was observed for the probe after reacting with citrate in the red channel (Fig. 6). The cell images in the bright field, red, and green channels were merged as shown in Figs. 6A–E. The Pearson's co-localization coefficient value was determined to be 0.95 through overlapping of the red and green images (Figs. 6B–D).

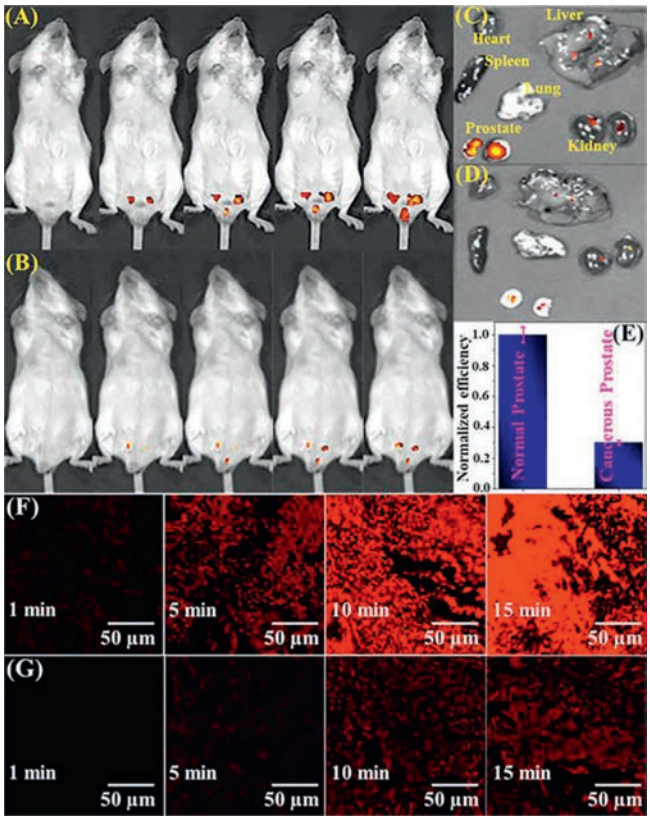

Fig. 7. Confocal images of Kunming mice administrated tail vein injection of **QIB** (500 µL, 30 µmol/L) for 0–15 min (A) non-cancerous; (B) prostate cancer. Dissection images of the heart, liver, spleen, lung, kidney, and prostate from mice (C) non-cancerous; (D) prostate cancer. (E) Quantitative evaluation of (C) and (D), reflecting fluorescence efficiency evolved from an area of interest around the prostate. Fluorescence images of resected prostate tissues using **QIB** (100 µL, 10 µmol/L) for 0–15 min (F) non-cancerous tissues and (G) cancerous tissues (excited at 514 nm; emitted at 535–590 nm).

Normal and cancerous Kunming mice groups were selected to examine citrate with *in vivo* models using **QIB**. The **QIB** probe (500 µL, 30 µmol/L) was injected into the tail vein of non-cancerous and cancerous mice to evaluate the concentration of citrate endogenously (*in situ*) in terms of the fluorescence intensity fluctuations over time from 0 to 15 min, as shown in Figs. 7A and B. The concentration of citrate in the non-cancerous mice was higher than that of cancerous mice; therefore, the fluorescence changes ranged from weak to strong red emissions for normal mice and extremely weak red emissions for cancer-affected mice (Fig. 7) [1,2]. Following this, the internal organs were dissected and imaged, and strong and weak red emissions on the prostate parts of the non-cancerous and cancerous mice in terms of citrate concentration, respectively, were observed (Figs. 7C and D). These results suggested that the concentration of citrate plays a significant role in the emission changes of the probe. These quantitative evaluation results are based on the relative fluorescence efficiency of the prostate organs, as shown in Fig. 7E. In addition, the prostate specimens were sliced and treated with the probe (100 µL, 10 µmol/L), observing a weak to strong red fluorescence over 15 mins for non-cancerous prostate tissues, as shown in Fig. 7F, whereas, cancer-affected prostate tissues had weak emissions in the red region (Fig. 7G), because the concentration of citrate was higher in the normal prostate compared with the cancerous prostate [1,2]. Moreover, other organ tissues of non-cancerous and cancerous mice were dissected and imaged, as shown in Figs. S11 and S12 (Supporting information). The data revealed that there were no obvious changes in the fluorescence of the probe even after a 15 min time duration.

The **QIB** probe demonstrated excellent selectivity, great water solubility, achievable sensitivity, strong red emission, and outstanding biocompatibility in detecting citrate biomolecules. Also, the probe achieved a possible reaction mechanism that was verified through ^{1}H NMR, HR-MS, and DFT. The practical utility of the probe was investigated in cell bioimaging, and showed mitochondria targeting ability. Next, quantitative measurements of citrate were performed using the non-cancerous and cancerous mice animal models, anatomized organs, and sliced prostate tissue imaging. Based on this, we envision that the probe can act as a feasible biochemical reagent for diagnosing PC assisted by healthcare centers and obtaining results for prevention and early stage treatment for PC patients. Since the normal prostate has higher citrate compared with that in the cancerous prostate, the cancer tissue with the surrounding normal tissue may observe a low or negligible fluorescence intensity. Thus, further investigations could be performed subject to these primary findings in clinical centers.

A newly designed **QIB** probe demonstrated Lewis acid–base and ICT sensing pathways for monitoring citrate in biological samples. The probe exhibited enhanced red emissions on reacting with citrate biomolecules. The properties of high water solubility and great biocompatibility can promote the extended application of **QIB** in biological experiments. Also, the probe secured mitochondria targeting ability for the detection of citrate in living cells. A quantitative evaluation of citrate was performed in animal models, anatomized organs, and sliced prostate tissues to distinguish the non-cancerous and cancerous mice by recording intense and weak red emissions, respectively. Therefore, we believe that **QIB** can perform as a reliable bio-analytical reagent in clinical centers to diagnose PC and treat it at an earlier stage based on our findings.

Declaration of competing interest

The authors declare that they have no known competing financial interests.

Acknowledgments

This work was financially supported by the National Natural Science Foundation of China (No. 22150410327) and the Basic Science Research Program through the National Research Foundation of Korea (NRF) funded by the Ministry of Science, ICT & Future Planning (No. 2020R1A2C1102741).

Supplementary materials

Supplementary material associated with this article can be found, in the online version, at doi:10.1016/j.cclet.2023.108880.

References

[1] S. Muthusamy, K. Rajalakshmi, P. Kannan, et al., Sens. Actuator. B: Chem. 369 (2022) 132299.
[2] K. Rajalakshmi, Y.S. Nam, M. Selvaraj, et al., Sens. Actuator. B: Chem. 259 (2018) 90–96.
[3] S. Mishra, E.S. Kim, P.K. Sharma, et al., ACS Appl. Bio. Mater. 3 (2020) 7821–7830.
[4] S. Bhagat, S. Singh, ACS Appl. Bio. Mater. 3 (2020) 3999–4011.
[5] X. Filella, L. Foj, Int. J. Mol. Sci. 17 (2016) 1784.
[6] K. Rajalakshmi, T. Deng, S. Muthusamy, et al., Spectrochim. Acta Part A: Mol. Biomol. Spectrosc. 268 (2022) 120622.
[7] J. Zhao, X. Dong, X. Hu, et al., Sci. Rep. 6 (2016) 22386.
[8] M.A. Schroeder, H.J. Atherton, D.R. Ball, et al., FASEB J. 23 (2009) 2529–2538.
[9] F. Ling, X. Tang, H. Zhang, et al., Biotechnol. Lett. 43 (2021) 1455–1466.
[10] A.U. Igamberdiev, Mitochondrion 52 (2020) 218–230.
[11] D. Granchi, N. Baldini, F.M. Ulivieri, R. Caudarella, Nutrients 11 (2019) 2576.
[12] V. Iacobazzi, V. Infantino, Biol. Chem. 395 (2014) 387–399.
[13] Z. Köstereli, K. Severin, Org. Biomol. Chem. 13 (2015) 252–257.

[14] Z. Zhu, J. Zhou, Z. Li, et al., Sens. Actuator. B: Chem. 208 (2015) 151–158.
[15] C. Liu, Y. Hang, T. Jiang, et al., Talanta 178 (2018) 847–853.
[16] C. Zhang, L. Han, Q. Liu, et al., Spectrochim. Acta Part A: Mol. Biomol. Spectrosc. 253 (2021) 119561.
[17] X. Chen, Z. Chen, Y. Hu, et al., Tetrahedron Lett. 100 (2022) 153870.
[18] X.B. Xu, Y.Y. He, et al., Dye. Pigment. 201 (2022) 110194.
[19] Y. Feng, S. Chi, G. Gao, et al., Sens. Actuator. B: Chem. 282 (2019) 16–26.
[20] X. Wang, T. Li, C. Ma, J. Hazard. Mater. 413 (2021) 125384.
[21] D.H. Ahn, J.W. Song, J. Comput. Chem. 42 (2021) 505–515.
[22] S. Jo, M. Ahn, K. Bhattarai, et al., Chem. Phys. Lett. 761 (2020) 138023.
[23] S. Refaely-Abramson, S. Sharifzadeh, M. Jain, et al., Phys. Rev. B 88 (2013) 81204.